302 *KSME International Journal, Vol. 16 No. 3, pp. 302~309, 2002*

Grid-Based Localization of a Mobile Robot Using Sonar Sensors

Jong-Hwan Lim*, Chul-Ung Kang
Faculty of Mechanical, Energy and Production Engineering, Cheju National University, Cheju-do 690-756, Korea

This paper presents a technique for localization of a mobile robot using sonar sensors. Localization is the continual provision of knowledges of position that are deduced from its a priori position estimation. The environment of a robot is modeled by a two-dimensional grid map. We define a physically based sonar sensor model and employ an extended Kalman filter to estimate positions of the robot. Since the approach does not rely on an exact geometric model of an object, it is very simple and offers sufficient generality such that integration with concurrent mapping and localization can be achieved without major modifications. The performance and simplicity of the approach are demonstrated with the results produced by sets of experiments using a mobile robot equipped with sonar sensors.

Key Words : Localization, Mobile Robot, Grid Map, Extended Kalman Filter

1. Introduction

To navigate a mobile robot autonomously, the mobile robot should have an ability to estimate its position to answer for "Where am I ?". Localization and relocation are two different scenarios for position estimation. The former is a continual provision of a knowledge of position which is deduced from its a priori position estimation (Leonard and Durrant-White, 1992; Kang and Lim, 1999), while the latter is the direct measurement of the position in a way that is independent of assumptions about previous movements (Drumheller, 1987; Lim and Leonard, 2000; Lim, 2001). Between the two scenarios, localization is the most crucial problem because it is required for every movement of the robot, while relocation is necessary for error recovery when the robot gets lost for long-term navigation.

* Corresponding Author,
E-mail : jhlim@cheju.ac.kr
TEL : +82-64-754-3712; **FAX** : +82-64-756-3886
Faculty of Mechanical, Energy and Production Engineering Cheju National University, Cheju 690-756, Korea. (Manuscript **Received** March 26, 2001; **Revised** December 21, 2001)

Cox (1991) suggested a localization method by using infrared range scanner and an odometer. Position updates are produced by a matching algorithm using an initial estimate of vehicle position from the odometer to launch an iterative registration procedure. Hinkel et al. (1988) and Hoppen et al. (1990) presented a localization technique that is performed from histogram using high-speed laser range scanner. Both of these were successful for a simple geometry environment such as corridors. But they would seem to have limited application with sonars because of sonars' slow data acquisition speed and the dissimilarity of sonar data to optical rangefinder data.

Elfes (1987) developed a method of position estimation based on sonar data. Positions are estimated by finding the best position that minimizes the discrepancy between reference and local grid maps. The limitation of this approach is that it cannot be applied to continuous position estimation because it is rather relocation than localization.

The problem of localization using sonar was first considered by Leonard and Durrant-White (1992). They developed a model-based

localization in which the model is composed of four geometric primitives (corner, edges, cylinders, and walls), and the position is estimated using an extended Kalman filter and regions of constant depth (RCDs) which are extracted from row sonar range data. Successful results are claimed for an indoor environment. However, some limitations restrict the applicability of the approach to a real world. Since the feature-based map building method is not yet successful, it can be hardly applied to an unknown environment.

The other limitation comes from the geometric representation of the environment. As mentioned in the Leonard's work (Leonard and Durrant-White, 1992), the matching between RCDs and a feature is performed differently for each geometric primitive, so that the procedure is very complex, and densely scanned data are required. Also, narrow cracks between two objects or small projecting parts of objects that are sensitive to sonar sensing may deteriorate the performance of the approach. It is because, if these parts belonging to a line target are not modeled, they can preclude to get consistent range returns from the target. As a result, RCDs from the target will not be available.

In this study, a grid-map-based localization is presented. Position is continuously estimated by using matching between a priori grid map and row sonar data. The approach is similar to the feature-based localization where it also utilizes an extended Kalman filter and a reference map given in advance. There are, however, three major differences : The first is that the approach in this paper is based on a grid map, so that the representation of a reference map and the matching procedure are very simple and easy because it does not require the exact geometric representation of an object. The second is that map updating is possible for grid-based map when the environment is changed, which is not yet successful for the feature-based map. This implies the localization method in this paper can be applied when the environment is changed. The third is that unlikely to Leonard's approach, it uses the row sonar data themselves, so that it can work even when only spare sonar data are available. It can be, therefore, a solution of concurrent mapping and localization that is the final goal of a mobile robot navigation.

2. Sensor Modeling

In this study, we consider ultrasonic sensors that are cheap and easy to use. A grid-based map is composed of 2-D occupancy grids that represent the occupied space by objects. Since inside of an object or empty space cannot give any information on the position, only the boundary of the object is represented by the occupancy grids in order to minimize the use of memory.

Figure 1 shows the sensor model of the approach based on a sonar sensor. In the figure, the vector $(x_s, y_s, \theta_s)^T$ contains information on the position and bearing of the sonar sensor respectively, and β the effective beam width of the sensor. Actual sonar sensing mechanism is a function of the wavelength, incidence angle of the beam, and surface roughness of the object. In specular wavelength regime, rough surface diffraction can be ignored because the surface of an object in an indoor environment is smooth in relation to the wavelength of the sonar (Bozma and Kuc, 1991a). Bozma and Kuc (1991b) found that with short and impulsive excitation the beam pattern of the Polaroid transducer has a Gaussian shape and minimized side-lobe effects.

Accordingly, we consider, in this paper, a very

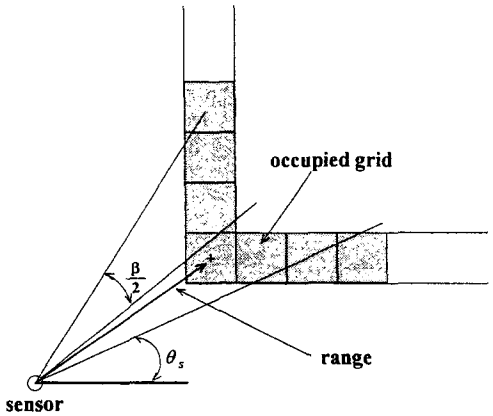

Fig. 1 Measurement modeling

simple sonar measurement model for convinice. That is, any occupied grid within the effective beam width (β) of the sensor can produce a range return as shown in Fig. 1. If there is more than one grid, the nearest grid from the sensor location is considered to give the range return because the sensor will detect only the first echo of the reflected beam.

3. Localization

The basic tool of the approach to localization is the extended Kalman filter. Kalman filtering techniques have been used extensively in location estimation problems such as missile tracking and ship navigation. The Kalman filter relies on the mathematical models of the employed plant and measurement.

3.1 The plant model

The plant model represents how the position $\mathbf{X}(k)$ of the robot changes with time in response to a control input $\mathbf{U}(k)$ in the presence of a disturbance $\mathbf{V}(k)$. With reference to Fig. 2, the position and orientation of the robot at time k is denoted by the state vector $\mathbf{X}(k)=[x(k), y(k), \theta(k)]^T$ defined with respect to a global coordinate frame. The general form of the position $\mathbf{X}(k+1)$ is

$$\mathbf{X}(k+1)=\mathbf{f}(\mathbf{X}(k), \mathbf{U}(k))+\mathbf{V}(k), \mathbf{V}(k)\sim N(0, \mathbf{Q}(k)) \quad (1)$$

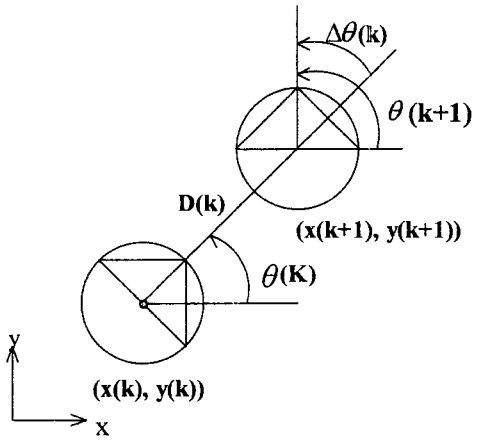

Fig. 2 Position and orientation of the robot at time step k and k+1

where, $\mathbf{f}(\mathbf{X}(k), \mathbf{U}(k))$ is a nonlinear state transition function, and $\mathbf{V}(k)\sim N(0, \mathbf{Q}(k))$ represents the noise source of zero-mean white Gaussian with covariance $\mathbf{Q}(k)$ (Gelb, 1973).

The model used here is based on Leonard's approach (Leonard and Durrant-White, 1992). The control input $\mathbf{U}(k)=(D(k), \Delta\theta(k))^T$ is a translation forward through the distance $D(k)$ followed by a rotation through the angle $\Delta\theta(k)$. Then the state transition function $\mathbf{f}(\mathbf{X}(k), \mathbf{U}(k))$ has the following form (Smith and Cheeseman, 1987)

$$\mathbf{f}(\mathbf{X}(k), \mathbf{U}(k))=\begin{bmatrix} x(k)+D(k)\cos\theta(k) \\ y(k)+D(k)\sin\theta(k) \\ \theta(k)+\Delta\theta(k) \end{bmatrix} \quad (2)$$

We call Eq. (2) as a point kinematic model, which has been proven adequate by through experiments as long as $D(k)$ is small.

3.2 Measurement model

When the robot is equipped with n sonar sensors, the measurement model $m_i(k)$ relates the observation of the i-th sensor to the robot's position and target (occupied grid) that produces the observation, and has the form

$$m_i(k)=g_i(\mathbf{X}(k), \mathbf{T})+h_i(k), h_i(k)\sim N(0, R_i(k)) \quad (3)$$

where $\mathbf{T}$ represents the target, and $h_i(k)$ indicates measurement noise that is assumed to be zero mean white Gaussian with covariance $R_i(k)$. The target $\mathbf{T}$ indicates the occupied grids within the beam width of the sensor i, and has the form

$$\mathbf{T}=\{(x_{ij}, y_{ij}) | 0\le j\le r\} \quad (4)$$

where r is the total number of occupied grids within the beam width.

As shown in Fig. 3, if we let $[x'_s, y'_s, \theta'_s]^T$ be the position of a sensor i in the robot coordinate frame, each sensor position $[x_s(k), y_s(k), \theta_s(k)]^T$ with global coordinate frame is expressed as follows:

$$\begin{pmatrix} x_s(k) \\ y_s(k) \\ \theta_s(k) \end{pmatrix}=\begin{pmatrix} x(k)+x'_s\cos(\theta(k))-y'_s\sin(\theta(k)) \\ y(k)+x'_s\sin(\theta(k))-y'_s\cos(\theta(k)) \\ \theta(k)+\theta'_s \end{pmatrix} \quad (5)$$

Accordingly, using the sensor model described in Section 2, $g_i(\mathbf{X}(k), \mathbf{T})$ can be expressed as

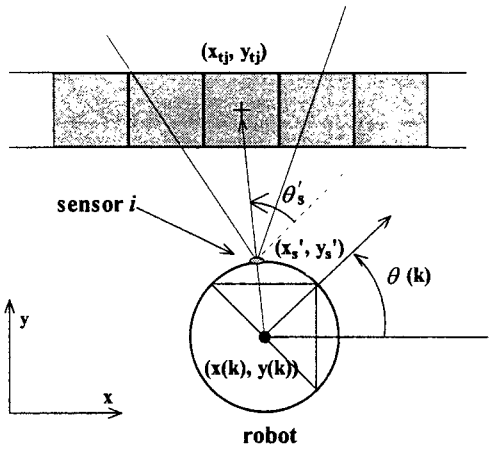

Fig. 3 Global and local sensor locations

$$g_i(k)=\min\{\sqrt{(x_s(k)-x_{tj}(k))^2+(y_s(k)-y_{tj}(k))^2}\mid 1\le j\le r\}. \quad (6)$$

If there is no occupied grid within the beam width, $g_i(k)$ has the maximum detection range of the sensor.

3.3 Position estimation

The goal of localization is to compute the new a posteriori position estimate $\hat{\mathbf{X}}(k+1\mid k+1)$ along with its covariance $\mathbf{C}(k+1\mid k+1)$ which is given by the a posteriori position estimate $\hat{\mathbf{X}}(k\mid k)$, its covariance $\mathbf{C}(k\mid k)$ for time k, the current control input $\mathbf{U}(k)$, and the current set of observations $\{m_i\mid 1\le i\le n\}$. Using the plant model and the control input $\mathbf{U}(k)$, the new location at time step $k+1$ is predicted such that

$$\hat{\mathbf{X}}(k+1\mid k)=\mathbf{f}(\hat{\mathbf{X}}(k\mid k),\mathbf{U}(k)). \quad (7)$$

The covariance $\mathbf{C}(k+1\mid k)$ associated with this prediction is (Gelb, 1973) given by

$$\mathbf{C}(k+1\mid k)=\nabla\mathbf{f}\mathbf{C}(k\mid k)\nabla\mathbf{f}^{\mathrm{T}}+\mathbf{Q}(k) \quad (8)$$

where $\nabla\mathbf{f}$ is the Jacobian of the state transition function $\mathbf{f}(\hat{\mathbf{X}}(k\mid k),\mathbf{U}(k))$. By linearizing Eq. (2) about the updated state estimate $\hat{\mathbf{X}}(k\mid k)$, we get

$$\nabla\mathbf{f}=\begin{bmatrix}1 & 0 & -\hat{D}(k)\sin\hat{\theta}(k\mid k)\\ 0 & 1 & \hat{D}(k)\cos\hat{\theta}(k\mid k)\\ 0 & 0 & 1\end{bmatrix} \quad (9)$$

where $\hat{D}(k)$ is evaluated by dead reckoning.

The next step is to predict observations $\hat{m}_i(k+1)$ from each sensor considering the position estimate $\hat{\mathbf{X}}(k+1\mid k)$. From the measurement model described in Section 3.2, we get

$$\hat{m}_i(k+1)=g_i(\hat{\mathbf{X}}(k+1\mid k),\mathbf{T}). \quad (10)$$

The innovation $\nu_i(k+1)$ is, then, defined to match the actual sensor measurement $m_i(k+1)$ and the predicated observation $\hat{m}_i(k+1)$ corresponding to the same sensor i as follows:

$$\begin{aligned}\nu_i(k+1)&=m_i(k+1)-\hat{m}_i(k+1) \quad (11)\\ &=(m_i(k+1)-g_i(\hat{\mathbf{X}}(k+1\mid k),\mathbf{T}))\end{aligned}$$

and related innovation covariance $s_i(k+1)$ is (Bar-Shalom and Fortmann, 1988) given by

$$s_i(k+1)=\nabla\mathbf{g}_i\mathbf{C}(k+1\mid k)\nabla\mathbf{g}_i^{\mathrm{T}}+\mathbf{R}_i(k+1) \quad (12)$$

where the Jacobian of observation $\nabla\mathbf{g}_i$ is computed by Eqs. (5) and (6),

$$\nabla\mathbf{g}_i=\begin{bmatrix}\frac{1}{d}(\hat{x}_s(k)-x_{tj})\\ \frac{1}{d}(\hat{y}_s(k)-y_{tj})\\ (x_{tj}-\hat{x}_s(k))(x'_s\sin(\theta(k+1\mid k))+y'_s\cos(\hat{\theta}(k+1\mid k)\\ +(y_{tj}-\hat{y}_s(k))(-x'_s\cos(\theta(k+1\mid k))+y'_s\sin(\hat{\theta}(k+1\mid k)))\end{bmatrix}^{\mathrm{T}} \quad (13)$$

In Eq. (13), d is the distance from the predicted sensor location to the target grid, and j is the index of the nearest occupied grid from the sensor i. In order to determine the correspondence between measurements and predictions, the following validation gate is used (Leonard and Durrant-White, 1992)

$$\nu_i(k+1)s_i^{-1}(k+1)\ \nu_i^{\mathrm{T}}(k+1)\le e^2 \quad (14)$$

where e is a design parameter. If Eq. (14) holds we can get a successful match.

The last step for localization is to use successfully matched observations and predictions to compute the updated robot location estimate, $\hat{\mathbf{X}}(k+1\mid k+1)$. For valid measurements $m_i(k+1)$ and predictions $\hat{m}(k+1)$, the composite innovation is computed to form $\nu(k+1)$ by

$$\nu(k+1)=\begin{bmatrix}m_1(k+1)-\hat{m}_1(k+1)\\ \vdots\\ m_j(k+1)-\hat{m}_j(k+1)\end{bmatrix} \quad (15)$$

where j is the total number of validated sets of

measurements and predictions that satisfy Eq. (14). In addition, the measurement Jacobian $\nabla \mathbf{g}_i$ for each validated measurement is stacked together to form the composite measurement Jacobian $\nabla \mathbf{g}$ as follows:

$$\nabla \mathbf{g} = \begin{bmatrix} \nabla \mathbf{g}_1 \\ \vdots \\ \nabla \mathbf{g}_j \end{bmatrix} \quad (16)$$

Using a stacked noise vector $\mathbf{R}(k+1) = \text{diag}[\mathbf{R}_i(k+1)]$, the composite innovation covariance $\mathbf{S}(k+1)$ is computed from Eq. (12), that is,

$$\mathbf{S}(k+1) = \nabla \mathbf{g} \mathbf{C}(k+1 \mid k) \nabla \mathbf{g}^T + \mathbf{R}(k+1). \quad (17)$$

Then, the well-known Kalman gain $\mathbf{W}(k+1)$ can be written as (Bar-Shalom and Fortmann, 1988)

$$\mathbf{W}(k+1) = \mathbf{C}(k+1 \mid k) \nabla \mathbf{g}^T \mathbf{S}^{-1}(k+1). \quad (18)$$

With Eq. (18), we can compute the updated robot position estimate

$$\hat{\mathbf{X}}(k+1 \mid k+1) = \hat{\mathbf{X}}(k+1 \mid k) + \mathbf{W}(k+1) \nu(k+1), \quad (19)$$

and the associated covariance

$$\mathbf{C}(k+1 \mid k+1) = \mathbf{C}(k+1 \mid k) - \mathbf{W}(k+1) \mathbf{S}(k+1) \mathbf{W}^T(k+1). \quad (20)$$

4. Experimental Verification

To illustrate the usefulness of the localization method with a real robot, the algorithm was run by off-line using data obtained from precisely known position. Figure 4 shows the configuration of a Nomad Scout robot equipped with ring of 16 Polaroid sonar sensors spaced at 22.5° angular intervals. Due to the restriction in the robot communications software, the range resolution of the sonar data is 0.025m and the detection ranges are 0.15m to 10m.

The experimental environment is composed of walls, papers boxes, book shelves, radiator, and triangular shaped object made of metal as shown in Fig. 5. The room model was measured by hand. Vehicle motion was guided at the PC by an operator specifying forward, left turn, and right turn commands in discrete steps, usually 0.3m or 10 degrees. The robot was run about 60m making five complete runs around the environment. A "stop, look, move" run is adopted in this experiment. In each discrete step, we first measured the robot's position and orientation by hand. Then 16 sonar range data and dead reckoning data were acquired from the robot. Since the ground in the room was very smooth, we added process noise shown in Table 1 artificially

Table 1 Error characteristics

	translation (1m)		rotation (1°)	
	mean	σ	mean	σ
x(m)	0.005	0.04(e_{tt})	0.0	0.01(e_{rt})
y(m)	0.005	0.04(e_{tt})	0.0	0.01(e_{rt})
θ(°)	0.0	0.05(e_{tr})	0.05	0.05(e_{rr})

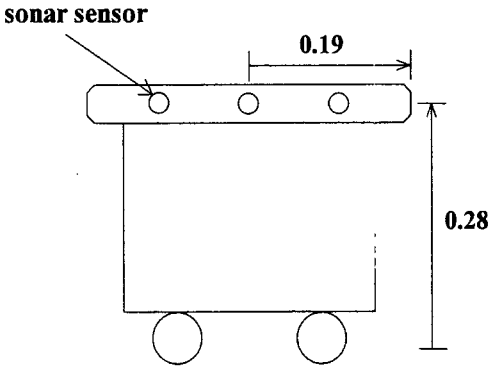

Fig. 4 Configuration of the Nomad Scout robot (unit : m)

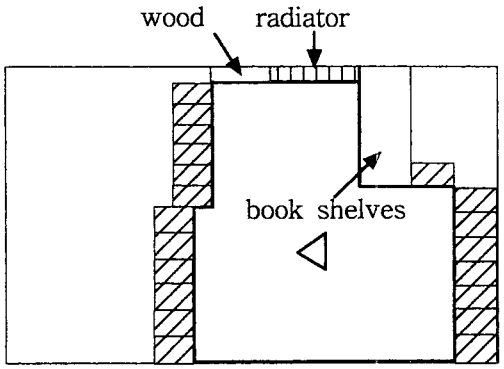

Fig. 5 Model of the room for localization. The thick lines and dashed rectangles represent the out line of the experimental environment and paper boxes, respectively

to the odometric position values in order to make unfavorable conditioned environment. The robot was, then, moved to the next position determined arbitrarily by the operator. We performed these sequence for 165 positions. In doing this, no position control or path planner was adopted.

A value of 2 was used for the validation gate in Eq. (14), 10 degrees for the effective beam width (β) of the sonar, and $0.02m^2$ for R_i. Each component of the matrix $\mathbf{Q}(k)$ is given in Table 1 assuming un-correlated Gaussian noise and point kinematics in order to reflect standard deviations of 4 centimeters of position error and 4.5 degrees of orientation error for each meter of translation and 90 degrees of rotation, respectively. At the starting position, perfect knowledge about the initial position is available for the robot.

In the experiments, a ring of fixed sonars was used. The advantage of the ring of a fixed sonar is that a set of returns over a wide spread of orientations can be quickly obtained. However, interpreting the data is made more difficult because each range measurement has no local support, e.g., RCDs, as in the densely sampled scan (Leonard and Durrant-White, 1992). Also, there were lots of unmodeled geometric primitives such as small cracks and projecting parts that give strong returns in sonar sensing. These two can seriously deteriorate the performance of the localization.

We have tested the localization method for various size of grids. Figure 6 shows the experimental results for grid size of $0.04 \times 0.04 m^2$. In the figure, rectangle, solid triangle, and dotted triangle represent true, estimated and odometric positions of the robot, respectively. The estimated errors for each step are plotted in Fig. 7. The maximum position error and orientation error are 0.051m and 5°, and the root mean square error for position and orientation are 0.022m and 3°, respectively. Looking at the figures, one can find the dead reckoning error tends to diverge as the traveling distance is increased, but the localization error is conversed regardless of the long traveling distance.

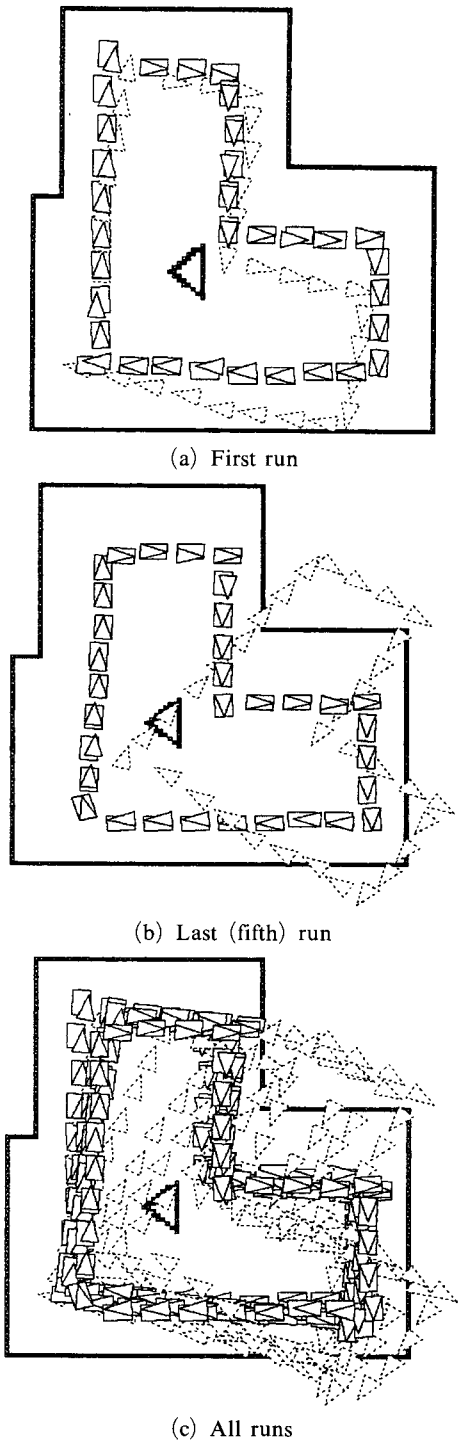

(a) First run

(b) Last (fifth) run

(c) All runs

Fig. 6 Experimental results. Rectangle, triangle, and dotted triangle represent true, estimated, and odometric positions, respectively

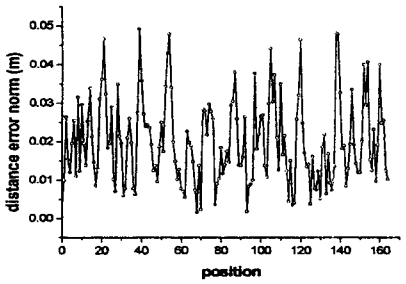

(a) Distance error to the true position

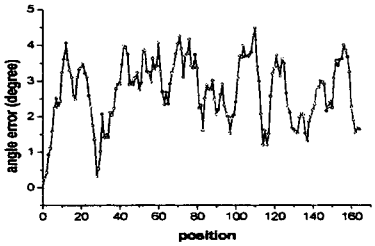

(b) Angle error to the true orientation

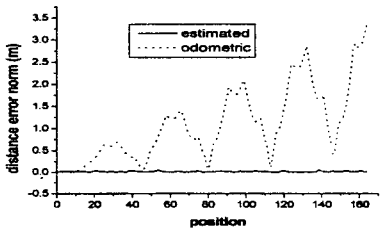

(c) Estimated error vs. odometric error (distance)

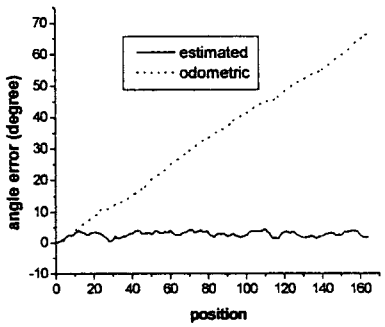

(d) Estimated error vs. odometric error (degree)

Fig. 7 Plots of estimated error and odometric error to the true positions

Table 2 shows the effect of the grid size on the localization results. As the grid size decreases the localization error is also decreased. The time required for one step of localization, however, was increased because the number of occupied grid for range prediction was also increased.

Table 2 Effect of the grid size

Grid size (mxm)		0.02 × 0.02	0.04 × 0.04	0.06 × 0.06	0.08 × 0.08
Error (m)	rms	0.021	0.022	0.028	0.054
	σ ($\times 10^{-2}$)	0.032	0.034	0.031	0.081
	max	0.046	0.051	0.062	0.147
Angle error (°)	rms	2.7	3.0	3.1	4.3
	σ	0.020	0.023	0.022	0.038
	max	4.3	5.0	4.9	6.7
Time/step (sec)		0.034	0.009	0.004	0.002

5. Conclusions

Localization of a mobile robot using a grid map has been developed and tested with real data obtained in an indoor environment. The experimental results were fairly good for a practical application. A grid-based map is easy to represent the environment comparing with a feature-based map, so that the localization procedure is very simple. It is because, for the feature-based map, exact geometric shapes of objects are required and each geometric primitive (e.g., plane, corner or edge, cylinder) should be considered in a different way for localization procedure. This is why the feature-based localization has limited applications to concurrent mapping and localization (CM&L).

In contrast to the feature-based localization, grid-based localization does not require an exact geometric shape of an object. Since a grid is basically a point target, the approach does not need to model narrow cracks or small projecting part of an object that are bothersome, or not easy to model. Also, the algorithm presented in this paper does not attempt to extract RCDs from densely sampled sonar scan. Instead, it uses the range returns themselves to estimate positions of the robot. We, therefore, believe that the approach in this paper offers sufficient generality such that integration with concurrent mapping and localization can be achieved without major modifications. The related work will include tests of the performance for the approach to an environment in which only a part of the environment

is known in advance.

References

Bar-Shalom, Y. and Fortmann, T. E., 1988, *Tracking and Data Association*, Academic Press.

Bozma, O. and Kuc, R., 1991a, "Characterizing Pulses Reflected from Rough Surfaces Using Ultrasound," *Journal of Acoustical Society of America*, Vol. 89, No. 6, pp. 2519~2531.

Bozma, O. and Kuc, R., 1991b, "Building a Sonar Map in a Specular Environment Using a Single Mobile Transducer," *IEEE Trans. Pattern Analysis and Machine Intelligence*, Vol. 13, No. 12, pp. 1260~1269.

Cox, I. J., 1991, "Blanche - an Experiment in Guidance and Navigation of an Autonomous Robot Vehicle," *IEEE Trans. Robotics and Automation*, Vol. 7, No. 3, pp. 193~204.

Drumheller, M., 1987, "Mobile Robot Localization Using Sonar," *IEEE Trans. Pattern Analysis and Machine Intelligence*, Vol. 9, No. 2, pp. 325~332.

Elfes, A., 1987, "Sonar-Based Real-World Mapping and Navigation," *IEEE Trans. Robotics and Automation*, Vol. 3, No. 3, pp. 249~265.

Gelb, A. C., 1973, *Applied Optimal Estimation*, The MIT Press.

Hinkel, R., Knieriemen, T. and Puttkamer, E., 1988, "Mobot-III an Autonomous Mobile Robot for Indoor Applications," Preceedings of the *International Symposium and Exhibition on Robots*, Sydney, Australia.

Hoppen, P., Knieriemen, T. and Puttkamer, E., 1990, "Laser-Radar Based Mapping and Navigation for an Autonomous Mobile Robot," *Proc. IEEE Int. Conf. Robotics and Automation.*

Kang, S. K. and Lim, J. H., 1999, "Sonar Based Position Estimation System for an Autonomous Mobile Robot Operating in an Unknown Environment," *KSME International Journal*, Vol. 13, No. 4, pp. 339~349.

Leonard, J. J. and Durrant-White, H. F., 1992, *Direct Sonar Sensing For Mobile Robot Navigation*, Kluwer Academic Publisher.

Lim, J. H. and Leonard, J. J., 2000, "Mobile Robot Relocation from Echolocation Constraints," *IEEE Trans. Pattern Analysis and Machine Intelligence*, Vol. 22, No. 9, pp. 1035~1041.

Lim, J. H., 2001, "Relocation of a Mobile Robot Using Sparse Sonar Data," *KSME International Journal*, Vol. 15, No. 2, pp. 217~224.

Smith, R. and Cheeseman, P., 1987, "On the Representation and Estimation of Spatial Uncertainty," *International Journal of Robotics Research*, Vol. 5, No. 4, pp. 56~68.